Journal Name

ARTICLE

A Self-assembly Route to Porous Polyaniline/Reduced Graphene Oxide Composite Materials with Molecular-level Uniformity for High-performance Supercapacitors†

Received 00th January 20xx,
Accepted 00th January 20xx

DOI: 10.1039/x0xx00000x

www.rsc.org/

Jifeng Wu,[a,c] Qin'e Zhang,[a] Jingjing Wang,[a] Xiaoping Huang,[a] and Hua Bai* [a,b]

Polyaniline/graphene composites constitute an important class of electrode materials for supercapacitors. In this paper, we designed a new self-assembly method for preparing polyaniline/reduced graphene oxide three-dimensional porous composite gels with molecular-level uniformity even at very high PANI content (> 80%). The method involves two successive self-assembly processes, namely, two-dimensional assembly of polyaniline on graphene oxide sheets in water/*N*-methyl-2-pyrrolidone blend solvent, and three-dimensional reduction-assembly of the obtained polyaniline/graphene oxide composite sheets. The prepared polyaniline/reduced graphene oxide composite gels possess a three-dimensional porous network composed of reduced graphene oxide sheets, which are covered by polyaniline thin coating with controlled thickness. Because of this favorable microstructure, the composite shows high specific capacitance of 808 F g^{-1} (5717 mF cm^{-2}) at a current density of 53.33 A g^{-1} (377.4 mA cm^{-2}), as well as excellent rate performance. These results demonstrate that two-step self-assembly is a promising method for precisely controlling the microstructure of reduced graphene oxide based composite electrode materials.

Introduction

Electrochemical energy storage is a key technology for clean and sustainable mobile energy supply. In this regard, electrochemical supercapacitors have aroused great interest for their potential applications in various areas, such as electric vehicles, mobile electronic products, and uninterrupted power supply.[1,2] Among various electrode materials for electrochemical supercapacitors, polyaniline (PANI) has attracted substantial attention, because of its low cost, good environmental stability, fast and reversible doping/dedoping kinetics.[3,4] The unique doping mechanism of PANI brings a high charge density on the backbone, thus PANI has a high specific capacitance.[5-7] Recent report has demonstrated that by incorporating reduced graphene oxide (RGO) into PANI to increase the specific surface area and electric conductivity, a high specific capacitance of 777 F g^{-1} can be achieved at a current density of 1 A g^{-1}.[8] So far as now, PANI/RGO has become the most-investigated material the among various conducting polymer composites suitable for supercapacitors.

Conventional methods of preparing PANI-based electrode materials usually involve *in-situ* polymerization of aniline on current collector or other substrates, such as RGO matrix.[8–11] Although many high-performance PANI-based electrode materials have been prepared *via in-situ* polymerization and related methods, there are obvious shortages of these methods.[12] A major one is that in *in-situ* polymerization it is difficult to precisely control the morphology and component distribution of PANI-based materials. For example, highly porous RGO hydrogel is an excellent conductive matrix for PANI, but *in-situ* polymerization of aniline on this porous RGO matrix, either chemical or electrochemical, will yield a non-uniform PANI coating.[11,13] The competition between diffusion and polymerization in porous substrate makes the deposition of PANI difficult to control. From a performance point of view, a porous and uniform molecular-level blend of PANI and RGO is preferred, while the non-uniform distribution of PANI may cause blockage of pores and the consequent undesired concentration polarization in the electrode.[11] Preparing such a molecular-level blend of PANI and RGO in electrode, however, is still a big challenge.

Self-assembly in solution is efficient way to precisely control the composition of a composite.[14,15] PANI has good solubility in several organic solvents,[16] but there are very few wet methods for fabricating PANI electrode, possibly because the solution-assisted processing method is difficult to produce PANI nanostructure, which is essential to high capacitive performance. Herein, by taking graphene oxide (GO) as a two-dimensional (2D) surfactant to disperse PANI, we develop a facile and controllable method of preparing nanostructured PANI/RGO composite gel (PGG) with molecular-level uniformity,

[a] College of Materials, Xiamen University, Xiamen, 361005, China, P.R. Email: baihua@xmu.edu.cn
[b] Graphene Industry and Engineering Research Institute, Xiamen University, Xiamen, 361005, China, P.R.
[c] Department of Physics, Fudan University, Shanghai, 200433, China, P. R.; Institute of Natural Sciences, Westlake Institute for Advanced Study, Westlake University, Hangzhou 310064, China, P. R.

† Electronic Supplementary Information (ESI) available: some supplementary pictures, characterizations, and comparison of PGG with other electrode materials.

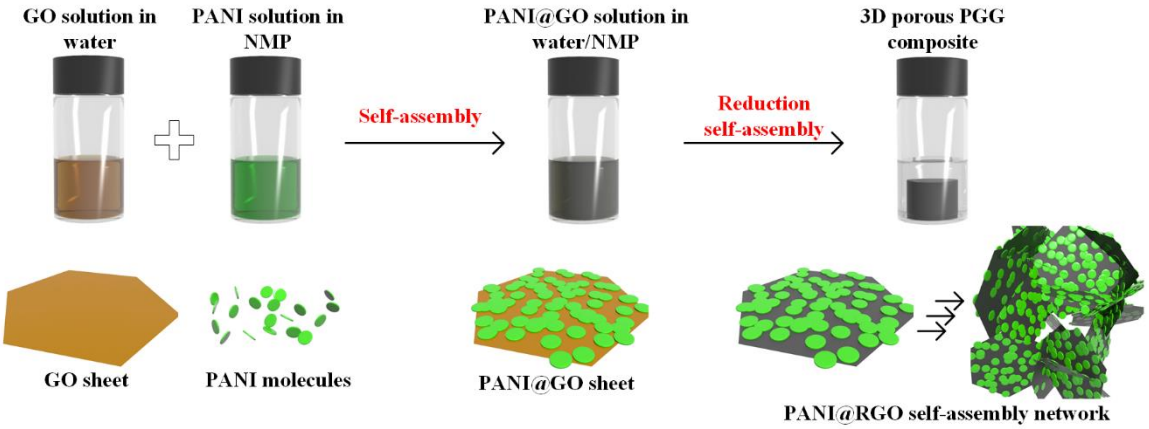

Fig. 1. Schematic illustration of solution-based self-assembly method for preparation of PGGs.

based on a solution-assisted two-step self-assembly strategy. The first self-assembly occurred between PANI and GO, when PANI solution in *N*-methyl-2-pyrrolidinone (NMP) was mixed with GO dispersion in water; it led to PANI@GO composite nanosheets dispersed in NMP/water blend solvent. Then the GO component was reduced into RGO, and the produced PANI@RGO nanosheets underwent a second self-assembly, forming PGG. In PGG there is a 3D porous network, consisting of a RGO self-assembling skeleton on which PANI was coated uniformly at molecular level. Because of this favorable microstructure, PGGs show an impressive specific capacitance of 824 F g^{-1} (5830 mF cm^{-2}) at 2.22 A g^{-1} (15.72 mA cm^{-2}) in 1 M H_2SO_4 aqueous electrolyte, and excellent rate performance (98% capacitance retention from 2.22 A g^{-1} to 53.33 A g^{-1}).

Results and discussion

The two-step method for preparing PGG is schematically illustrated in Fig. 1. Firstly, PANI solution in NMP was mixed with GO solution in water, yielding a blend solution of PANI@GO in the mixed solvent. Then the blend solution was treated with ascorbic acid at 90 °C for 2 hours, and converted into a gel, as shown in Fig. 2A. The residual solution around the gel was nearly colorless (Fig. S1A), indicating that all the GO and PANI had entered the gel. Therefore, the content of PANI in PGG can be easily controlled by the feeding ratio of PANI and GO. When the PANI feeding ratio was 37.5%, 54.5%, 60%, 66.7%, 75% or 81.8% (by weight), the final PANI content in the prepared PGG was 58.3%, 71.8%, 75.8%, 81.3%, 87.1% and 91.0%, as calculated by weight measurement, and these PPGs are referred to as PGG-1, -2, -3, -4, -5, and -6, respectively. Raman, infra-red (IR) spectra and X-ray photoelectron spectrum (XPS) (Fig. S2 ~ S4) confirm that PGGs were composed of PANI and RGO. Scanning electron microscopy (SEM) images reveal that all the lyophilized PGGs (aerogel) have an interconnected three-dimensional (3D) network (Fig. 2). The 3D porous structure provides channels for the diffusion of electrolyte, thus is benefit for high rate performance.[11,17,18] With the increase in the PANI content, the morphology of the network changed slightly. The network of PGG-1 is composed with 2D nanosheets, similar with that of pure RGO hydrogels (RGOHGs). The nanosheets are smooth and uniform, and no large PANI particle is observed on these nanosheets, indicating that PANI distributes evenly on the RGO sheets. As the content of PANI was increased, the thickness of PANI layer on the RGO sheets became thicker (Fig. 2 B, C and D). When the content of PANI reached 81.3%, the nanosheets in PGG-4 were curled (Fig. 2C). Similar curled sheets were also observed in PVA/GO aerogels,[19] and are caused by the imbalanced surface tension on two sides of polymer-covered nanosheets. Further increasing PANI content led to large aggregates in the PGG (Fig. 2E), because of the too low dispersibility of PANI@GO composite sheets at large PANI content.

According to the above results, the formation mechanism of PGG was proposed. PANI has good solubility in NMP, but is insoluble in water. When water is added into PANI solution in NMP, the PANI chains become less solvated, and thus they tend to absorb onto the GO sheets driven by the strong π-π interaction. This self-assembly produced PANI@GO composite nanosheets dispersed in the blend solvent. The PANI@GO dispersion is stable, because the polar oxygen-containing groups on GO have high affinity to the solvent (noticing that GO is also dispersible in NMP[20]). No sedimentation was observed even after the dispersion was stored for several weeks. If the PANI@GO dispersion was agitated at 3000 rpm for 10 min, a dark blue precipitate and colorless supernatant were obtained, showing that all the PANI chains had assembled onto GO sheets and thus entered the precipitate (Fig. S1B). Here GO sheets serve as 2D surfactant which can disperse PANI in the blend solvent. The formation of PANI@GO sheets was confirmed by atomic force microscopy (AFM), and transmission electron microscopy (TEM) images. The PANI@GO nanosheet (PANI feeding ratio: 66.7%) show a thickness of ~5 nm under AFM (Fig. 3A), larger than GO (~ 1 nm), and protuberances on the nanosheet and indicate the existence of PANI component. The magnified SEM images also clear demonstrate the rougher surface of PANI@GO, as compared with GO (Fig. S1CD). TEM images in Fig. 3B & C clearly reveal that PANI is loaded on GO

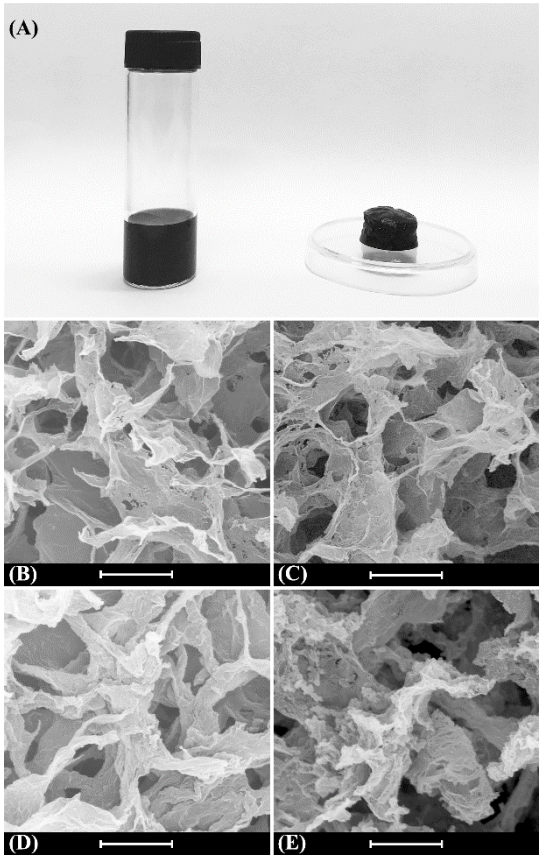

Fig. 2. Photograph and SEM images of PGGs. (A) Photographs of PANI@GO solution and PGG-4. (B) ~ (E) SEM images of lyophilized PGGs with different PANI content: (B) 58.3% (PGG-1), (C) 71.8% (PGG-2), (D) 81.3% (PGG-4) and (E) 91.0% (PGG-6). Scale bar: 5 μm.

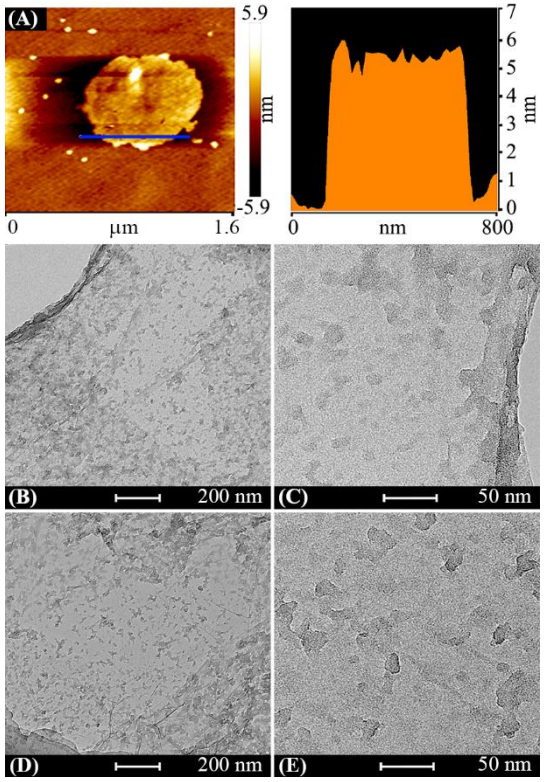

Fig. 3. Morphology of PANI@GO and PANI@RGO sheets. (A) AFM image of PANI@GO sheet. (B)(C) TEM of PANI@GO sheets. (D)(E) TEM of PANI@RGO sheets.

sheet as small nanoparticles, with average diameter of ~25 nm. These PANI nanoparticles are homogeneously distributed on GO sheets, and separated from each other spatially. Given that the molecular mass of our PANI is 19000 ~ 86000,[21] the diameter of single PANI molecule is calculated to be 12 ~ 55 nm (spherical particle with a density of 1.2 g cm^{-3}), in agreement with the size of PANI nanoparticles. Therefore, we can infer that most PANI nanoparticles contain only one PANI chain. This means that PANI chains are loaded GO sheets with a molecular-level uniformity.

When the oxygen-containing groups on GO sheets were removed by the reductant ascorbic acid, the PANI@GO composite sheets lose their dispersibility and assemble into a 3D network.[22] The of RGO sheets during reduction was widely used to prepare RGO gels,[23–26] and the present result confirmed that the self-assembly was not affected by the PANI coating. Control experiment reveals that no chemical reactions occur between emeraldine base and ascorbic acid under the same experimental condition. TEM images of PANI@RGO sheets in PGG-4 show that the size and shape of PANI nanoparticles were well preserved during the GO reduction (Fig. 3D, E). In fact, because the π-π interaction between PANI and GO becomes even stronger after the reduction of GO, as the conjugated areas on GO grow larger, the PANI nanoparticle on GO sheets is stable in the GO reduction process, and the PANI@GO composite sheet takes part in the 3D self-assembly as an entity. As a result, the PANI nanoparticles are preserved in the prepared PGG, and the porous composite of PANI/RGO with molecular-level uniformity was obtained.

The PGG monoliths have good mechanical strength, as demonstrated by the rheological data (Fig. S5). Thus, it is free-standing and can be directly used as electrode without any additive. Taking PGG-4 as an example, we investigated the performance of PGGs as the electrode of electrochemical supercapacitors. Fig. 4 shows the capacitive performance of PGG-4 (mass loading: 7.1 mg cm^{-2}) tested in a three-electrode system with 1 M H_2SO_4 as the electrolyte. The cyclic voltammogram (CV) curves of the PGG-4 at different scan rates (Fig. 4A) display a rectangular shape superimposed with a pair of redox peaks, indicating the coexistence of both the electrical double-layer capacitance and pseudocapacitance. The CV curves deform at high scan rate, because of large time constant ($\tau = RC$) caused by large capacitance and/or resistance, and pseudo-reversible kinetics of PANI redox. The specific capacitance of PGG-4 was measured by galvanostatic charge/discharge (GCD) technique. A high specific capacitance of 824 F g^{-1} (5830 mF cm^{-2}) is achieved at 2.22 A g^{-1} (15.72 mA cm^{-2}, Fig. 4B. For two electrode test, see Fig. S8). This value is among the highest specific capacitance of PANI/RGO composites in previous reports (See Table S1 for comparison).[11,27–43] The high specific capacitance is partly attributed to the degradation products of PANI. We have demonstrated in our earlier paper that the redox peaks at ~0.5 V is attributed to the hydroxyl or amino terminated oligoanilines,

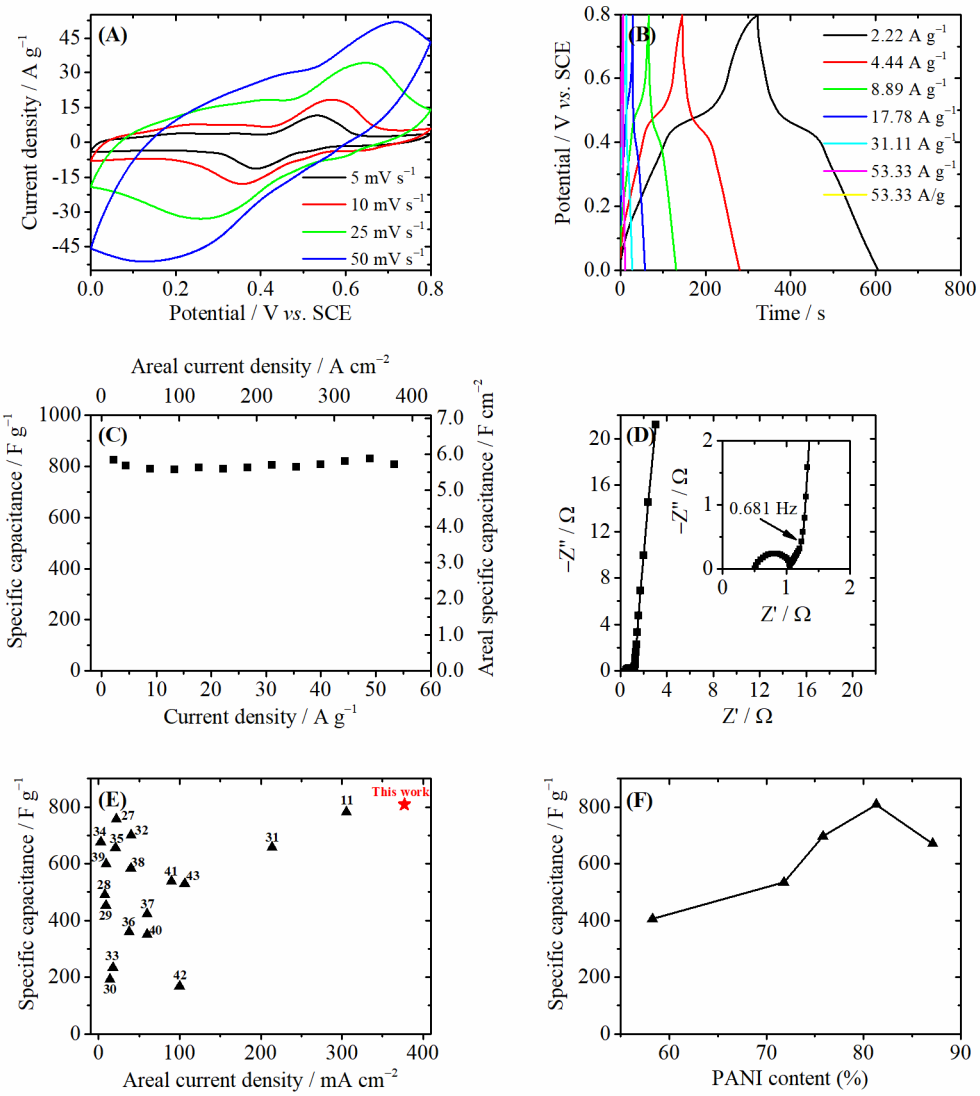

Fig. 4. Capacitive performance of PGG. (A) CV curves of PGG-4 at the scan rate of 5 mV s^{-1}, 10 mV s^{-1}, 25 mV s^{-1} and 50 mV s^{-1}. (B) GCD curves of PGG-4 at the different current density. (C) Specific capacitances of PGG-4 versus current densities. (D) Nyquist plots of PGG-4. (E) Comparison of the specific capacitances of PGG-4 and other PANI/RGO composite materials in literature. All the specific capacitance values are corresponding to the highest current density reported in literature. (F) Specific capacitance of PGGs (at ~ 40 A g^{-1}) versus PANI content in PGGs.

which are produced in-situ during the redox cycles and have large specific capacitance (> 1000 F g^{-1}).[6] With RGO network as a conductive matrix, hydroxyl or amino terminated oligoanilines can contribute a considerable part of the capacitance and significantly increase the total specific capacitance of the composite. The contribution of degradation products of PANI, however, always exists in any PANI/RGO composite electrode material. Thus, the superior specific capacitance of PGG-4 is also ascribed to its favorable microstructure. The uniform and small PANI nanoparticles on the RGO matrix are beneficial for the high capacitance, because all the PANI chains are rendered both accessible to electrolyte and close to RGO conductive matrix, so that there is little "dead mass" in the composites.

Nyquist plot in Fig. 4C shows the impedance of PGG-4 electrode in the frequency range of 100 kHz to 0.01 Hz. The equivalent series resistance (R_s) of the electrode, which can be suggested by the x intercept of the Nyquist plot, was 0.47 Ω. In the high-frequency region, the small semicircle indicates a small charge transfer resistance, which is ascribed to the fast kinetics of the redox of PANI and its degradation products. In the low-frequency part of the plot, when the frequency is lower than 0.681 Hz, the curve tends toward a vertical line, owing to semi-infinite diffusion. This result implies that the electrode shows almost ideal capacitive behavior. However, the PGG electrode suffers from a low cycling stability problem. The capacitance retention is about 73% after 5000 GCD cycles testing (Fig. S7). The main reason for the low cycling life is the continuous degradation of PANI at high electrode potential. This problem, however, can be solved by controlling the working potential range of the PANI/RGO electrode.[6]

PGG-4 has an excellent rate performance. Even at a very high current density of 53.33 A g^{-1} (377.4 mA cm^{-2}), the specific capacitance remains 808 F g^{-1} (5717 mF cm^{-2}). This means when the current density is increased by 24 times, the specific

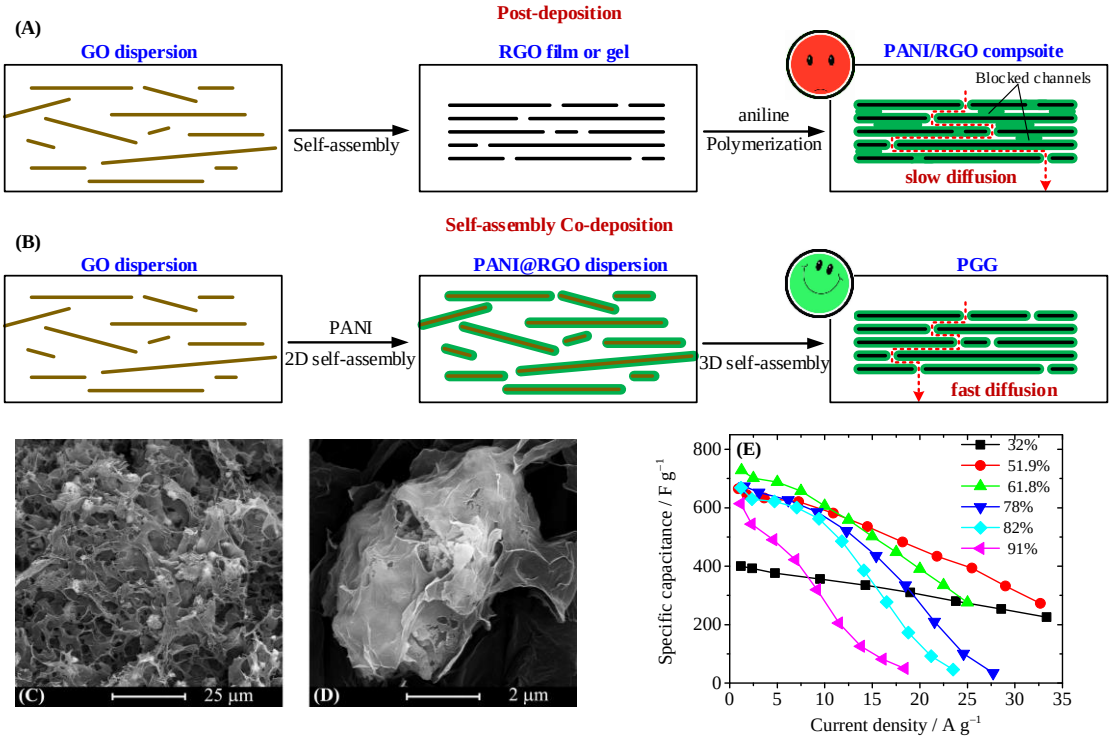

Fig. 5. (A) Schematic illustration of the formation of partially blocked channels in in-situ polymerization of aniline on RGO matrix. (B) Schematic illustration of the formation of unblocked channels in self-assembly process. (C) (D) SEM images of the PGG synthesized in water/DMSO blend solvent. (E) Specific capacitance of PGGs synthesized in water/DMSO blend solvent with different PANI feeding ratios.

capacitance retention is as high as 98%. Fig. 4E compares the specific capacitance of PANI-based materials measured at high current densities. It is shown that PPG-4 electrode can work at the highest areal current density in the literature, while the specific capacitance was among the highest values. (Also see Table S1 for comparison).[11,27–43] We ascribe the high rate performance to the small diameter of PANI particles and fast electrolyte diffusion inside the PGG. It has been demonstrated that the rate performance of PANI/RGO composite electrode strongly depends on the electrolyte diffusion rate, both inside the bulk PANI phase and in the whole porous electrode.[11] Thus, small PANI thickness is desired. Our self-assembly method ensures uniform loading of PANI on RGO sheets, even the PANI content is as high as 81.3%. As demonstrated by the TEM image in Fig. 3, the size of PANI nanoparticle in PGG-4 is only ~25 nm. Consequently, the diffusion of electrolyte in PANI phase is very fast.

Apart from the small size of PANI phase, the interconnected channels in PGG also enable fast diffusion of electrolyte inside the composite. The conventional methods of preparing PANI/RGO composites usually involve *in-situ* polymerization of aniline on RGO substrate (post-deposition strategy). In the RGO substrate, however, there are plenty of slit pores between 2D RGO sheets. These slit pores are easily blocked by the newly-deposited PANI, leading to slow electrolyte diffusion and low rate performance (Fig. 5A).[11] In our preparation method, PANI@GO nanosheets are the building blocks of the self-assembly which leads to PGG, and PANI is incorporated before the formation of slit pores in PGG (co-deposition strategy). Thus, PANI will not block the channels in PGG (Fig. 5B). That is the principle reason why PGG has excellent rate performance.

We also investigated the influence of PANI content on the capacitive performance of PGGs. It was found that all the PGG electrodes with different PANI content possess excellent rate performance (Fig. S6), because they all have unblocked channels for the fast diffusion of electrolyte. Fig. 4F shows the specific capacitance of different PGGs at the current density of 40 A g^{-1}. The specific capacitances of PGGs increase with the content of PANI, and reach maxima of 808 F g^{-1} at the PANI content of 81.3%. Obviously, more PANI bring larger contribution of pseudocapacitance. When the PANI content is increased to 87.1%, the specific capacitance declines to 671 F g^{-1}. A possible reason is that when the attached PANI film gets thicker and the RGO sheets become curled, as shown in Fig. 2, some PANI chains are not accessible to electrolyte. Finally, we are going to discuss the effect of the solvent of PANI solution on the preparation and the capacitive performance of PGG. Although NMP is one of the best solvents for PANI, there are many other solvents that can also dissolve PANI. Here we tried to use dimethyl sulfoxide (DMSO) to replace NMP in our self-assembly method. The SEM image in Fig. 5C and Fig. 5D show that in the prepared PGG there are plenty of PANI aggregates with size of several micrometers. A close observation indicates that the aggregates are composed of PANI short fibers, and some of the aggregates are wrapped by RGO sheets. (Fig. 5(D)). The formation of these fibril aggregates is caused by self-

assembly of PANI chains in the bulk DMSO/water solvent. When water is introduced into PANI solution, the formation of PANI nanofiber (homogeneous nucleation) and the absorption of PANI on GO sheet (heterogeneous nucleation) are two competing processes. Because the solubility of PANI in DMSO is relatively low, the nucleation of PANI is so fast that some of the PANI chains will nucleate homogeneously, yielding large aggregates. These aggregates reduce the rate performance of the composite, because of the slow electrolyte diffusion inside them. As shown in Fig. 5E, although all the samples have large specific capacitance at low current densities, their specific capacitances decrease rapidly with the increasing current density. The higher the content of PANI is, the larger and more the PANI aggregates are, and the faster the capacity drops with the current density. These results reveal the importance of a proper solvent to the self-assembly method, and they again confirm that small PANI particle size can promote the rate performance of composite electrodes.

Experimental

Materials

Aniline (AR), ammonium persulfate (AR), hydrogen peroxide (30%), hydrochloric acid (36%), NMP and sulfuric acid (H_2SO_4, 98%) were purchased from Sinopharm Chemical Reagent Co., Ltd, and used as received. GO was prepared by oxidation of natural graphite powder (325 mesh, Qingdao Huatai lubricant sealing S&T Co. Ltd.) according to a modified Hummers' method.[44] PANI was synthesized by chemical oxidation polymerization.[21] Briefly, aniline (9.313 g, 0.100 mol) was added to hydrochloric acid solution (100 mL, 1.0 M) and the pH adjusted to 1.0 by hydrochloric acid. Ammonium persulfate (28.52 g, 0.125 mol) was dissolved in pure water (51.5 mL) and added dropwise to the reaction solution which was being stirred at 0 °C. After 1 h the reaction product was recovered by filtration and washed with distilled water (10 × 200 mL). The product was then deprotonated by stirring for 24 h in aqueous ammonia solution (100 mL, 33%), filtered and washed with deionized water (2 x 200 ml) then with ethyl alcohol (2 × 200 mL), finally dried under vacuum at 60 °C for 24 h, yielding emeraldine base as dark blue powder.

Preparation of PGGs

PANI stock solution in NMP (30 mg mL^{-1}) was prepared by stirring emeraldine base in NMP for 4 h under 50 °C. To prepare PGG, 5 mL GO aqueous solution (2 mg mL^{-1}) containing 40 mg sodium ascorbate was mixed with different amount of PANI stock solution, and the homogeneous blend solution was heated at 90 °C for 2 h. After reaction, the as-produced gel was collected and dialyzed in pure water for 24 h to remove any impurities. RGO hydrogel was prepared by heating 5 mL GO aqueous solution (2 mg mL^{-1}) containing 40 mg sodium ascorbate at 95 °C for 1.5 h, and purified by dialysis in water for 24 h.

Electrochemical measurement

The capacitance performance of PGGs was investigated in three-electrode systems.[45] In all the electrochemical tests, 1 M H_2SO_4 was used as the electrolyte. For the test, a model supercapacitor device was assembled, with two platinum foils as the current collectors, and a piece of PGG as the working electrode, and another piece of RGO hydrogel as the counter electrode. The areal mass loading of the electrode was 5 ~ 7 mg cm^{-2}, unless specified otherwise. Before the setup of the device, the PGGs were immersed in the electrolyte overnight to exchange their interior water with the electrolyte. A saturated calomel electrode (SCE) was employed as the reference electrode. The specific capacitances of PGGs composites were calculated according to the following equation:

$$C_S = \frac{Jt}{\Delta V - IR}, \quad (1)$$

and

$$J = \frac{I}{m}, \quad (2)$$

where V is potential range of the GCD process, and m is the mass of the PGGs electrode; I is the current applied on the electrode, t is the discharge time, and IR represents the voltage drop at the beginning of the discharge process, caused by internal resistance of the system.

Characterization

All the electrochemical measurements were conducted on a CHI 660D electrochemical workstation (CHI, US). The morphology of the composites was observed using a SU-70 field emission scanning electron microscope (Hitachi, Japan) operated at 20 kV. Raman spectra were performed at room temperature with a MicroRaman System RM3000 spectrometer (Horiba, Japan) and an argon ion laser operating at a wavelength of 633 nm as the excitation. UV-Vis spectra were gained on the UV-2550 spectrometer (Shimadzu, Japan). XPS was collected on the PHI Quantum 2000 spectrometer (Quantum 2000, USA) using monochromated X-rays from an Al K source with a takeoff angle of 45° from the surface plane.

Conclusions

In summary, we designed a novel self-assembly method for preparing 3D porous PANI/RGO composite, which were used as the electrode materials for the high-performance supercapacitor. The self-assembly method includes two successive self-assembly processes, and 3D porous composites consisting of RGO framework and PANI thin coating with molecular-level uniformity were obtained. This favorable microstructure facilitates the diffusion of the electrolytes and transport of the electrons in the composites, thus high specific capacitance and excellent rate performance were achieved. These results indicate that two-step solution-based self-assembly is a promising method for preparing RGO composites for electrode materials. Also, it is confirmed that GO is an effective 2D surfactant, which can form complex with other molecules, and bring them into complicated self-assembly processes. This strategy may guide us to design other RGO-

based composite materials with various compositions, structures, and functions.

Conflicts of interest

There are no conflicts to declare.

Acknowledgements

This work was supported by Natural Science Foundation of China (21774104).

Notes and references

1 R. Kötz, M. Carlen, *Electrochim. Acta,* 2000, **45**, 2483.
2 L. Zhang, X. Zhao, *Chem. Soc. Rev.,* 2009, **38**, 2520.
3 J. Miller, A. Burke, *Electrochem. Soc. Interface,* 2008, **17**, 53.
4 P. Simon, Y. Gogotsi, *Nat. Mater.,* 2008, **7**, 845.
5 A. Rudge, I. Raistrick, S. Gottesfeld, J. Ferraris, *Electrochim. Acta,* 1994, **39**, 273.
6 Q. E. Zhang, A. A. Zhou, J. J. Wang, J. F. Wu, H. Bai, *Energy Environ. Sci.,* 2017, **10**, 2372.
7 C. Peng, D. Hu, G. Chen, *Chem. Commun.,* 2011, **47**, 4105.
8 K. Li, J. Liu, Y. Huang, F. Bu, Y. Xu, *J. Mater. Chem. A,* 2017, **5**, 5466.
9 Y. Yong, X. Dong, M. Chan-Park, H. Song, P. Chen, *ACS Nano,* 2012, **6**, 2394.
10 J. Xu, K. Wang, S. Zu, B. Han, Z. Wei, *ACS Nano,* 2010, **4**, 5019.
11 J. F. Wu, Q. E. Zhang, A. A. Zhou, Z. F. Huang, H. Bai, L. Li, *Adv. Mater.,* 2016, **28**, 10211.
12 L. Wang, X. Lu, S. Lei, Y. Song, *J. Mater. Chem. A,* 2014, **2**, 4491.
13 K. W. Chen, L. B. Chen, Y. Q. Chen, H. Bai, L. Li, *J. Mater. Chem.,* 2012, **22**, 20968.
14 Y. X. Xu, G. Q. Shi, *J. Mater. Chem.,* 2011, **21**, 3311.
15 G. Whitesides, B. Grzybowski, *Science*, 2002, **295**, 2418.
16 Y. Cao, J. Qiu, P. Smith, *Synth. Met.,* 1995, **69**, 187.
17 L. Zhang, G. Q. Shi, *J. Phys. Chem. C,* 2011, **115**, 17206.
18 Y. Hu, P. Adelhelm, B. Smarsly, S. Hore, M. Antonietti, J. Maier, *Adv.Funct. Mater.,* 2007, **17**, 1873.
19 H. Bai, C. Li, X. L. Wang, G. Q. Shi, *Chem. Commun.,* 2010, **46**, 2376.
20 J. Paredes, S. Villar-Rodil, A. Martínez-Alonso, J. Tascon, *Langmuir*, 2008, **24**, 10560.
21 P. M. Adams, P. J. Laughlin, A. P. Monkman, A. M. Kenwright, *Polymer*, 1996, **37**, 3411.
22 K. X. Sheng, Y. X. Xu, C. Li, G. Q. Shi, *New Carbon Mater.,* 2011, **26**, 9.
23 Y. X. Xu, Q. Wu, Y. Q. Sun, H. Bai, G. Q. Shi, *ACS Nano*, 2010, **4**, 7358.
24 H. Cong, X. Ren, P. Wang, S. Yu, *ACS Nano*, 2012, **6**, 2693.
25 W. Chen, S. Li, C. Chen, L. Yan, *Adv. Mater.,* 2011, **23**, 5679.
26 B. Choi, M. Yang, W. Hong, J. Choi, Y. Huh, *ACS Nano*, 2012, **6**, 4020.
27 M. Xue, F. Li, J. Zhu, H. Song, M. Zhang, T. Cao, *Adv. Funct. Mater*., 2012, **22**, 1284.
28 H. Cong, X. Ren, P. Wang, S. Yu, *Energy Environ. Sci.,* 2013, **6**, 1185.
29 C. Chang, Z. Hu, T. Lee, Y. Huang, W. Ji, W. Liu, J. Yeh, Y. Wei, *J. Mater. Chem. A,* 2016, **4**, 9133.
30 Z. Tong, Y. Yang, J. Wang, J. Zhao, B. Su, Y. Li, *J. Mater. Chem. A*, 2014, **2**, 4642.
31 D. Li, Y. Li, Y. Feng, W. Hu, W. Feng, *J. Mater. Chem. A,* 2015, **3**, 2135.
32 W. Li, H. Lu, N. Zhang, M. Ma, *ACS Appl. Mater. Interfaces,* 2017, **9**, 20142.
33 R. Wang, M. Han, Q. Zhao, Z. Ren, X. Guo, C. Xu, N. Hu, L. Lu, *Sci. Rep.,* 2017, **7**, 44562.
34 S. Giri, D. Ghosh, C. Das, *Adv. Funct. Mater.,* 2014, **24**, 1312.
35 N. Hu, L. Zhang, C. Yang, J. Zhao, Z. Yang, H. Wei, H. Liao, Z. Feng, A. Fisher, Y. Zhang, Z. Xu, *Sci. Rep.,* 2016, **6**, 19777.
36 Y. Xu, Y. Tao, X. Zheng, H. Ma, J. Luo, F. Kang, Q. Yang, *Adv. Mater.,* 2015, **27**, 8082.
37 P. Sekar, B. Anothumakkool, S. Kurungot, *ACS Appl. Mater. Interfaces,* 2015, **7**, 7661.
38 J. Yan, L. Yang, M. Cui, X. Wang, K. Chee, N. Viet Cuong, V. Kumar, A. Sumboja, M. Wang, P. Lee, *Adv. Energy Mater.,* 2014, **4**, 1400781.
39 P. Yu, X. Zhao, Z. Huang, Y. Li, Q. Zhang, *J. Mater. Chem. A,* 2014, **2**, 14413.
40 Y. Gawli, A. Banerjee, D. Dhakras, M. Deo, D. Bulani, P. Wadgaonkar, M. Shelke, S. Ogale, *Sci. Rep.,* 2016, **6**, 21002.
41 M. Yu, Y. Huang, C. Li, Y. Zeng, W. Wang, Y. Li, P. Fang, X. Lu, Y. Tong, *Adv. Funct. Mater.,* 2015, **25**, 324.
42 G. Xu, B. Ding, J. Pan, J. Han, P. Nie, Y. Zhu, Q. Sheng, H. Dou, *J. Mater. Chem. A,* 2015, **3**, 23268.
43 Y. Wang, X. Yang, L. Qiu, D. Li, *Energy Environ. Sci.* 2013, **6**, 477.
44 Y. Q. Chen, K. W. Chen, H. Bai, L. Li, *J. Mater. Chem*., 2012, **22**, 17800.
45 L. B. Chen, H. Bai, Z. F. Huang, L. Li, *Energy Environ. Sci*., 2014, **7**, 1750.